Available online at www.sciencedirect.com
SCIENCE DIRECT®
Journal of Sound and Vibration 266 (2003) 465–480
JOURNAL OF SOUND AND VIBRATION
www.elsevier.com/locate/jsvi

Determination of the dynamical behaviour of biological materials during impact using a pendulum device

M. Van Zeebroeck*, E. Tijskens, P. Van Liedekerke, V. Deli, J. De Baerdemaeker, H. Ramon

Department of Agro-Engineering and -Economics, Laboratory for Agro-Machinery and Processing, Catholic University Leuven, Kasteelpark Arenberg 30, 3001 Leuven, Belgium

Received 13 January 2003

Abstract

A pendulum device has been developed to measure contact force, displacement and displacement rate of an impactor during its impact on the sample. Displacement, classically measured by double integration of an accelerometer, was determined in an alternative way using a more accurate incremental optical encoder. The parameters of the Kuwabara–Kono contact force model for impact of spheres have been estimated using an optimization method, taking the experimentally measured displacement, displacement rate and contact force into account. The accuracy of the method was verified using a rubber ball. Contact force parameters for the Kuwabara–Kono model have been estimated with success for three biological materials, i.e., apples, tomatoes and potatoes. The variability in the parameter estimations for the biological materials was quite high and can be explained by geometric differences (radius of curvature) and by biological variation of mechanical tissue properties.

1. Introduction

Most mechanical injury of fruit is caused by mechanical impact that occurs during harvesting, handling and transportation. The fruit and vegetable industry suffers considerable economic losses due to bruising. In 2000 and 2001, the portion of second choice apples (apples with bruises) in Belgium was respectively 15% and 8%. The auction price for second choice apples in Belgium is 1/3 of the normal price. Knowing the economic value of 124 million euro (calculation based on mean apple price paid to growers in the years 2000 and 2001), a reduction of 10% in

*Corresponding author.
E-mail address: michael.vanzeebroeck@agr.kuleuven.ac.be (M. Van Zeebroeck).

0022-460X/03/$ - see front matter
doi:10.1016/S0022-460X(03)00579-0

second choice apples can lead to an increase in income of Belgium growers by 595 000 (2001) and 892 000 (2000) euro.

The general purpose of this research is to construct a computer model, based on the Discrete Element modelling (DEM) to simulate damage to fruit occurring during mechanical handling in the process chain from harvesting to consumer (see [1]). This should allow one to identify critical sections in the process chain, e.g., harvesting machine, sorting, transport, etc., and to provide guidelines to optimize the operation of the harvesting machine and eventually to design harvesting machines, handling units and cushioning materials with a low risk of damaging the product. This requires essentially two components: a contact force model, which can be considered as the constitutive equation of the DEM problem, and a bruise model predicting the amount of bruise as a function of the contact history. This paper reports on the experimental determination of the former component, i.e., the contact force model.

In principle, contact and impact problems are continuum mechanical problems. A body is deforming and eventually failing under quasi-static or dynamic loading. The correct mathematical formulation is given by a system of partial differential equations expressing conservation of mass, momentum and energy. Solving them leads to the displacements and stresses as a function of space and time. However, as fruit tissue is a material with a microstructure determined by the delicate cellular arrangement of cell walls, cell liquid and air voids, the constitutive equation relating stress to strain is in fact at best highly speculative. In many contact theories (e.g., the Hertzian contact, see [2]) the contact area is approximated as a point and the contacting bodies are treated as rigid bodies whose motion is described by Newton's equation for translational motion, and Euler's equation for rotational motion. As a consequence, the mathematical description is transformed into a set of ordinary differential equations of motion. In this setting the contact force can be approximately described as a function of the virtual overlap of the two impacting bodies, defined as the instantaneous distance between the initial contact points on the two bodies. This information is captured in the *contact force model*, which can be viewed as the constitutive equation of the system. It is a basic ingredient of any Discrete Element model. This paper describes an experimental technique to measure contact force and displacement during a normal impact, i.e., an impact in which the contact forces are collinear with the centres of mass of the two bodies. The two bodies used are, in this case, the fruit and a metal impactor. In principal, the method can be generalized to impact of other materials (packaging material, crates, machine parts). Given the functional form of a contact force model, the parameters of the model can be determined indirectly by solving an optimization problem.

The experimental device being used for measuring contact force and displacement during impact is a pendulum. It simultaneously determines the contact force, the displacement of the surface of the impacted body, and the displacement rate. A pendulum is a classical device to determine bruise susceptibility of fruit and potatoes [3–6].

The bruise susceptibility is determined by measuring bruise volume together with absorbed energy of the fruit. To a less extent, a pendulum has also been used to determine the parameters of a contact force model. E.g., Nigg et al. [7] determined the stiffness and damping factor in a non-linear viscoelastic contact force model by least square data fitting of the experimentally measured force-deformation during impact of shoe-soles with an impactor.

This paper is structured as follows. In Sections 2.1 and 2.2 the pendulum device is discussed in detail. In Section 2.3 the method for estimation of the contact force model parameters is

discussed. In Section 2.4, the experimental results are validated using a non-biological material, which does not fail. Section 3 applies these techniques to three biological materials, i.e., apples, potatoes, and tomatoes. Finally, some important conclusions are formulated in Section 4.

2. Methodology

2.1. Experimental setup

The pendulum consist of a 0.505 m long arm with an aluminium impactor of spherical shape (radius of curvature: 25 mm) at its tip (see Figs. 1 and 2). The impactor itself is attached to a force sensor (Dytran instruments 1051V3, sensitivity: 11 mV/N). At the same height an accelerometer is attached (PCB piezotronics 352C22, sensitivity: 10 mV/g). At the hinge of the pendulum arm an incremental optical encoder (Heidenhain RON 275) is mounted. The data signals of these three sensors are collected by a National Instrument PCI-MIO-16E-1 card and processed by a LABVIEW program.

Fig. 1. General view of pendulum device (scheme see Fig. 2).

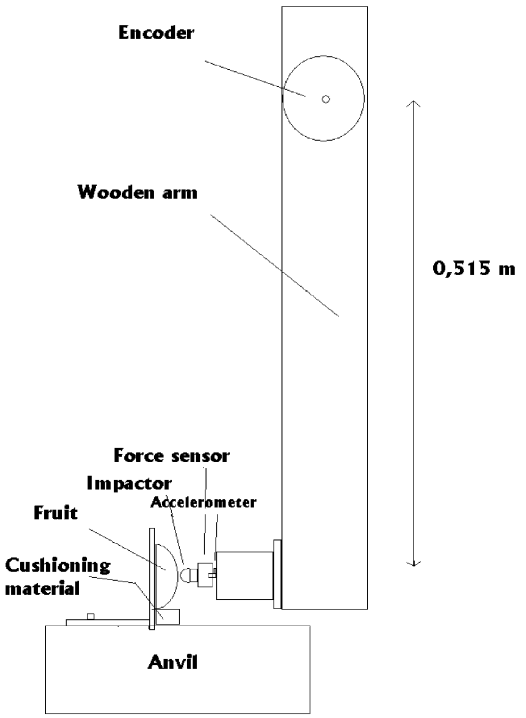

Fig. 2. Schematic representation of the pendulum arm and anvil. The positions of the different sensors and of the impacted body ("fruit") are indicated.

The sample to be tested (fruit for example) is attached to an anvil by an elastic band. The anvil is rigid enough to assume that its deflection or vibration is insignificant during impact. Round samples (apples, tomatoes and potatoes) are cut in two to minimize energy absorption at the contact surface of the anvil with the sample. By varying the initial angle of the pendulum arm, different impact energies can be created. The contact force $F_c(t_i)$ in the direction normal to the contact surface, displacement $x(t_i)$ and displacement rate $\dot{x}(t_i)$ of the impactor during impact are measured simultaneously, at the sampling times $t_i = t_0 + i/f$ $(i = 1, \ldots, n)$, with f the sampling frequency. t_0 and t_n denote the start and the end of the contact, respectively. Typically, $n \approx 1250$. The contact force $F_c(t_i)$ is measured by the force sensor. The acceleration $(\ddot{x}(t_i))$, measured by the accelerometer has been used as verification for the force sensor signal by taking in account the rotational inertia (I) and length (L) of the pendulum arm $(F_c(t_i) = (I/L)^2 \ddot{x}(t_i))$. Displacement and displacement rate are measured by an optical incremental encoder (details are provided in Section 2.2.), which in fact measures the angular position of the impactor. The tangential displacement of the impactor is calculated from the displacement angle by taking in account the length of the pendulum arm. The time of first contact of the impactor with the sample is detected by the force sensor. The rise in voltage (or corresponding force) beyond the noise level of the force sensor is detected. The noise level of the force sensor was quite high (~ 1 N). As a consequence, there is no data of the impact beneath 1 N (see Figs. 3–6). The displacement at the point of first contact of the impactor with the sample is equated to 0. Making use of the triggering point significantly

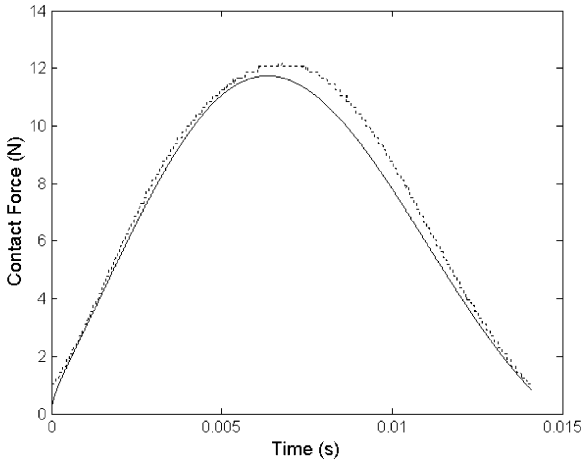

Fig. 3. Rubber: experimental and simulated contact force with parameter estimation based on displacement only. Solid line: simulation; Dotted line: experimental.

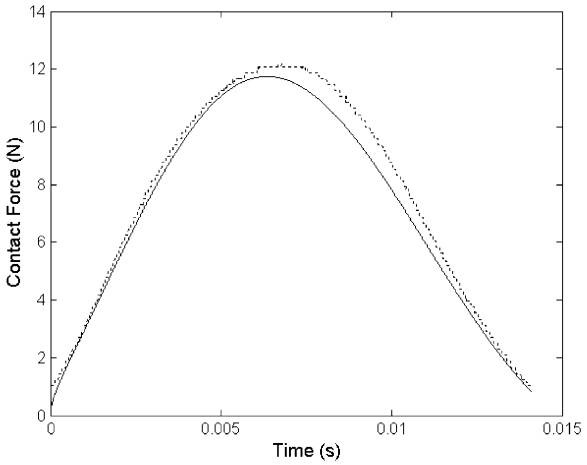

Fig. 4. Rubber: experimental and simulated contact force with parameter estimation based on displacement, displacement rate and contact force. Solid line: simulation; Dotted line: experimental.

decreases the calculation time of decoding the digital encoder signal (see Section 2.2.). The displacement rate of the impactor during impact is obtained from the instantaneous position as

$$\dot{x}_i = \frac{x_{i+1} - x_{i-1}}{2\delta t}, \tag{1}$$

with δt the time lapse between successive signals.

Absorbed energy is calculated by subtracting rebound energy of the impact. The impact and elastic energy are obtained from the calculated kinetic energy of the pendulum arm just before

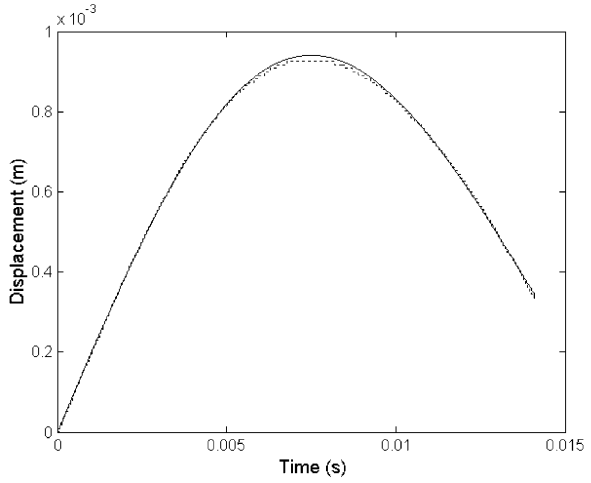

Fig. 5. Rubber: experimental and simulated displacement with parameter estimation based on displacement, contact force and displacement rate. Solid line: simulation; Dotted line: experimental.

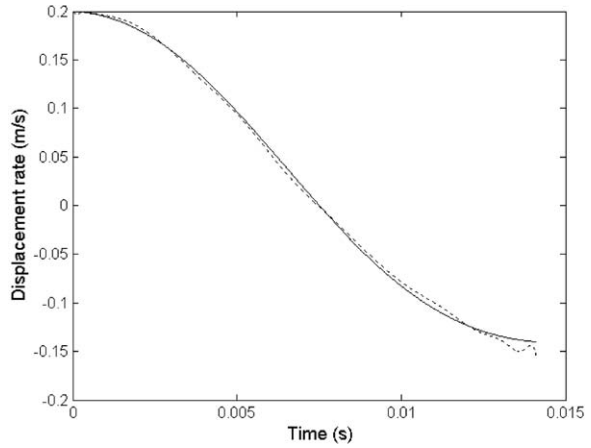

Fig. 6. Rubber: experimental and simulated displacement rate with parameter estimation based on displacement, displacement rate and contact force. Solid line: simulation; Dotted line: experimental.

and just after impact:

$$E_{impact} = E_{kin}(t_{-1}), \qquad E_{elastic} = E_{kin}(t_{n+1}), \qquad E_{absorbed} = E_{impact} - E_{elastic}. \tag{2}$$

t_{-1} and t_{n+1} denote the time of the final signal before impact, and the first signal after the impact, respectively. The kinetic energy is obtained as

$$E_{kin}(t) = \frac{1}{2} I\omega(t)^2 = \frac{1}{2} \frac{I\dot{x}(t)^2}{R^2}. \tag{3}$$

Here, ω is the angular velocity of the impactor. The impact and elastic energy have been calculated from the impact and rebound angle, which correspond in fact to potential energies [3,5,6]. An accurate determination of E_{impact}, $E_{elastic}$ and $E_{absorbed}$ is important for the bruise prediction model that will be treated in a following paper.

2.2. Experimental determination of displacement and displacement rate

In the literature, displacement rate and displacement are determined by integration and double integration respectively of an accelerometer signal. Several authors however have pointed out the inaccuracy of such numerical integration [8,9]. The reason is the uncertainty associated with the individual integration constants of the different frequencies in the signal. The use of highpass filtering can correct this effect to a certain extent. Highpass filtering is satisfactory when there is zero-mean displacement (vibration). When there is a non-zero mean displacement it can only be used for a short time interval (like impact), taking into account that the error on the integration still increases with time [9].

Instead of using the accelerometer, the displacement can be determined in a direct way by using an incremental optical encoder. The encoder sends out two digital signals (A and B) that are 90° phase-shifted. Each signal has a resolution of 18 000 cycles/rev (pulses/rev). The signals are electronically interpolated five times. This interpolation is integrated in the encoder itself. After analyzing the digital transitions of the two phase-shifted signals together in the LABVIEW program a resolution of 0.001° is achievable ($18\,000 \times 5 \times 4 = 360\,000$). The accuracy of the encoder, measured in the factory, is 0.0014°. Each signal (force sensor signal, encoder signal A and B) is sampled at a rate of 200 kHz, giving a temporal resolution of 5 μs. The time to switch between signal channels during data acquisition is at most 1 μs. This high sampling rate is necessary to avoid missing a transition of the encoder signal at the point of maximum velocity (just before impact). As all the signals are measured at a sampling rate of 5 μs a force–deformation curve could be constructed by plotting force against displacement measurements.

Comparison of the displacement–time and displacement rate–time curves calculated from the accelerometer signal (with high-pass filtering) with the displacement–time and displacement rate–time curves calculated from the encoder signal, confirmed that the displacement and displacement rate calculated from the accelerometer signal are less accurate. Especially at the end of the impact, the displacement rate and displacement are underestimated.

Due to the nature of numerical integration, displacement rate and displacement evolutions obtained from the accelerometer are much smoother than displacement rate and displacement measured by the encoder. As a consequence, the encoder is more susceptible to small fluctuations in displacement rate and displacement during impact than the accelerometer. A final advantage of the encoder as compared to the accelerometer, is that calibration is no longer needed.

2.3. Estimation of contact force model parameter

As explained in Section 2.1, the experimental data consists of the normal contact force $F_c(t_i)$, the displacement of the impactor $x(t_i)$ and the displacement rate $\dot{x}(t_i)$, at the sampling times t_i ($i = 1, \ldots, n$). Normal contact force models are generally expressed as a function of displacement,

x, and displacement rate, $\dot{x}$, and a number of parameters p_j ($j = 1, 2, \ldots$):

$$F_c^* = \gamma F_c^*(x, \dot{x}; p_1, p_2, ...), \tag{4}$$

γ is a geometric factor accounting for the radii of curvature of the colliding bodies. For the applications discussed in the remainder of the paper, γ is taken to be a constant, and is integrated in the parameters p_j^*. Since the materials used in the reported experiments can be approximated as viscoelastic spheres, the appropriate model is that of Kuwabara and Kono [10] and Brilliantov et al. [11]. In an approach similar to the original approach of Hertz for contact between perfect elastic spheres, they derived the following contact force for viscoelastic spheres:

$$F_c^* = -kx^{3/2} - cx^{1/2}\dot{x}. \tag{5}$$

The spring constant k is the same as that of the Hertz theory and the damping constant c is connected to the radii of curvature of the spheres and the two coefficients of bulk viscosity. Taguchi [12] reported that the factor $x^{1/2}$ copes with unphysical predictions of contact force models with linear damping, as e.g., in the Kelvin–Voigt model:

$$F_c^* = -kx - c\dot{x}. \tag{6}$$

In reality, at the start of impact, the contribution of the damping to the contact force F_c^* is zero, there the Kelvin–Voigt model predicts a finite value. The parameters p_j, k and c are estimated from the experimental data by minimizing an error function that is measuring the difference between the experimental data and predictions based on the contact force model (4). The equation of motion for the impactor is given by

$$I\ddot{\theta} = -mgr \sin\theta - F_c^* r \cos\theta. \tag{7}$$

θ is the angle between the arm of the impactor and the direction of gravity. The direction of the angle θ is so that $\dot{\theta}$ is positive during loading. The impacted object is positioned so that $\theta(t_0) = 0$. Furthermore, m, I and r are the mass, inertia and length of the pendulum arm, and g is the gravitational acceleration. The contact force F_c is given by Eq. (4) during contact, and vanishes after contact is lost. The displacement x during contact is related to the angle θ by $x = r \sin\theta$ and can generally be approximated by $\theta \cong x/r$, since θ is close to zero. The equation of motion (7) is easily solved by an explicit Runge–Kutta (4,5) formula (Matlab routine ode45).

The parameter estimation is carried out using a least squares non-linear data fitting technique (routine lsqnonlin of the Matlab optimisation toolbox). The technique effectively minimizes the cost function,

$$C = w_x \sum_i (x(t_i) - x^*(t_i))^2 + w_{\dot{x}} \sum_i (\dot{x}(t_i) - \dot{x}^*(t_i))^2 + w_F \sum_i (F_c(t_i) - F_c^*(t_i))^2, \tag{8}$$

with respect to the parameters of the contact force model. The cost function (8) measures the distance between experimental data and the solution of the equation of motion (7), which is denoted by the asterisk. The weights w_x, $w_{\dot{x}}$ and w_F can be chosen to vary the relative importance of the corresponding experimental quantities ($x(t_i)$, $\dot{x}(t_i)$ and $F_c(t_i)$).

Table 1
Different cost functions to estimate the contact force model parameters k and c in Eq. (5)

Experimental quantity	Cost function
Displacement $x(t_i)$ $(i = 0, \ldots, n)$	$C_x = w_x \sum_i (x(t_i) - x^*(t_i))^2$
Displacement rate $x(t_i)$ $(i = 0, \ldots, n)$	$C_{\dot{x}} = w_{\dot{x}} \sum_i (\dot{x}(t_i) - \dot{x}^*(t_i))^2$
Contact force $F_c(t_i)$ $(i = 0, \ldots, n)$	$C_F = w_F \sum_i (F_c(t_i) - F_c^*(t_i))^2$
Displacement, displacement rate	$C_{x\dot{x}} = w_x \sum_i (x(t_i) - x^*(t_i))^2 + w_{\dot{x}} \sum_i (\dot{x}(t_i) - \dot{x}^*(t_i))^2$
Displacement, contact force	$C_{xF_c} = w_x \sum_i (x(t_i) - x^*(t_i))^2 + w_F \sum_i (F_c(t_i) - F_c^*(t_i))^2$
Displacement rate, contact force	$C_{\dot{x}F_c} = w_{\dot{x}} \sum_i (\dot{x}(t_i) - \dot{x}^*(t_i))^2 + w_F \sum_i (F_c(t_i) - F_c^*(t_i))^2$
Displacement, displacement rate, contact force	$C_{x\dot{x}F_c} = w_x \sum_i (x(t_i) - x^*(t_i))^2 + w_{\dot{x}} \sum_i (\dot{x}(t_i) - \dot{x}^*(t_i))^2 + w_F \sum_i (F_c(t_i) - F_c^*(t_i))^2$

Weights are either zero or given by $w_q = 1/\langle q \rangle$.

2.4. Validation of experimental methodology

2.4.1. Optimization using the pendulum device

In order to validate the experimental methodology, the use of a test material with predictable behaviour is mandatory. Biological materials are to be avoided, because their behaviour is subject to many factors, which are still poorly understood. They exhibit biological variability—that is keeping obvious factors[1] constant, properties can still vary significantly, their state is not constant over time, etc. The material chosen was rubber. Its stiffness is of the same order of magnitude as for the biological materials under study, it does not show biological variability, and it does not yield. A rubber sphere (radius of curvature: 41.5 mm) was cut into two equal parts and one part was mounted on the anvil. A pendulum impact experiment with an initial drop angle of 10° has been repeated 20 times.

The parameters, k and c, of the Kuwabara–Kono model (5) were estimated for each repetition.

In the cost function (8) the weights w_x, $w_{\dot{x}}$ and w_F were chosen to normalize the different terms ($w_q = 1/\langle q \rangle$). In this way, each experimental quantity realizes an equal influence on the parameter estimation. Besides the repeatability of the measuring method, differences in the cost function were analyzed.

Seven different cost functions have been tried out to estimate the contact force model parameters, based on the possible combinations of the experimental quantities (contact force, displacement and displacement rate). They are described in Table 1.

The results of the parameter estimations for these different cost functions are given in Table 2. When the parameter optimization was carried out on contact force or displacement and respectively the displacement and contact force were calculated according to the optimized parameters, a good fit was found between the experimental and calculated displacement and contact force respectively. This is shown in Fig. 3, where the experimental force is compared to the

[1] Obviously, biological materials are generally not prepared in a controlled way. E.g., apples harvested at the same, even from the same tree, may have a very different history in terms of growth conditions and therefore can exhibit a wide variability for material properties. The obvious factors refer to the conditions which are under the control of the experimenter, such as harvesting time, storage conditions, conditions in the experimental setup, etc.

Table 2
Parameter estimation for a rubber ball for the Kuwabara–Kono contact force model (5) using different experimental quantity combinations

Cost function (see Table 1)	$\langle k \rangle \pm \sigma_k$ ($\mathrm{N\,m^{-3/2}}$)	$\langle c \rangle \pm \sigma_c$ ($\mathrm{kg\,m^{-1/2}\,s^{-1}}$)	Residual norm C^2
Displacement C_x	$391\,057 \pm 2893$	725 ± 29	$0.1*10^{-3} \pm 0.03*10^{-3}$
Displacement, displacement rate $C_{x\dot{x}}$	$394\,927 \pm 3000$	688 ± 12	111 ± 7
Displacement rate $C_{\dot{x}}$	$394\,933 \pm 3001$	688 ± 12	111 ± 7
Displacement, displacement rate, contact force $C_{x\dot{x}F_c}$	$394\,931 \pm 2990$	681 ± 11	121 ± 7
Displacement rate, contact force $C_{\dot{x}F_c}$	$394\,921 \pm 2993$	681 ± 11	121 ± 7.4
Displacement, contact force C_{xF_c}	$411\,653 \pm 2919$	549 ± 10	3.17 ± 0.29
Contact force C_{F_c}	$411\,679 \pm 2900$	549 ± 10	3.17 ± 0.29

calculated force when the optimization was carried out on displacement only. The fact that two independent devices (force sensor and encoder) lead to approximately the same result is encouraging.

However, quantitatively, the difference between parameter estimation based on displacement and parameter estimation based on contact force seems to be more pronounced. When the optimization is carried out for displacement and contact force separately, there is a difference of $176\,\mathrm{kg\,m^{-1/2}\,s^{-1}}$ in damping constant (28%) and $20\,622\,\mathrm{N\,m^{-3/2}}$ in spring constant (5%) between the optimization methods. The difference in damping constant is quite high.

The standard deviation of the damping parameter estimated by the different combinations of the experimental quantities ranged 1.6–1.8% (except for the optimization based on experimental displacement the standard deviation was 4%). The standard deviation of the spring constant ranged 0.7–0.8%. The measurement error on the spring and damping constants are acceptable.

We prefer to use the 'three experimental quantity optimization' in future analysis. When the three experimental quantities are used, the measurement error on force sensor and encoder in the results become less important. Figs. 4–6 compare respectively experimental and optimized displacement, displacement rate and contact force for an optimization using the three experimental quantities together. The conclusion is that the optimization of the contact force model is satisfactory when the displacement and displacement rate are considered (see Figs. 5 and 6). When the contact force is considered (Fig. 4), the optimization seems to be less satisfactory, but still acceptable.

In principle the contact force model parameters can also be estimated using the linear regression procedure.

$$Y = kX_1 + cX_2 \tag{9}$$

with

$$Y = F_c^*, \qquad X_1 = x^{*3/2}, \qquad X_2 = (x^*)^{1/2}\dot{x}^*.$$

The difference with the optimization technique is that it is only applicable on condition that all three experimental quantities x^*, $\dot{x}^*$ and F_c^* are available. The optimization method can still be used if one or two of these experimental quantities are missing.

2.4.2. Validation of the optimization technique using a universal testing machine (UTS)

2.4.2.1. Description of the device. The universal testing machine being used is the UTS-5 manufactured by UTS testsystheme GmbH. The rubber ball was placed on a stationary horizontal plate. A horizontal cross-head moves the second horizontal plate down ward with a pre-defined speed. A force sensor with a range of 0–200 N and a resolution of 0.001 N is placed between the cross-head and the second horizontal plate. A computer measures and controls the speed of the motor. By tracking the measuring time continuously the displacement can be calculated at every time-step. By plotting the force and the displacement at the same time-step a force–deformation curve can be constructed.

2.4.2.2. Measurement. The rubber ball was compressed at a constant deformation rate of 0.00017 m/s (= 10 mm/min) and 0.0017 m/s (100 mm/min) until the force of 170 N was reached. The maximum deformation was 4.1 mm. Because the noise of the force sensor signal in the low force region is too high, only that part of the force–deformation curve above a deformation of 2 mm was used for further analysis. The force–deformation curves are highly reproducible.

The force–deformation curves of two different measurements with a deformation rate of 0.00017 and 0.0017 m/s were analyzed using MATLAB. Linear regression was used to determine the parameters k and c in the Kuwabara–Kono model (5). The parameters obtained were $k = 733\,809\ \mathrm{N/m^{3/2}}$ and $c = 1078\ \mathrm{kg\,m^{-1/2}\,s^{-1}}$.

To compare these parameters with the parameters estimated with the pendulum device a recalculation was done using extended Hertz theory. According to Hertz theory, contact force parameters for the contact between a flat-plate and a sphere (in the case of the UTS) and contact between two spheres (in the case of the pendulum) are different. The theoretical calculation of this difference is given here. As mentioned in Kishino and Thornton [13] and Johnson [2] the normal force is given by

$$F = \frac{4}{3}E^*\sqrt{R^*}\delta^{3/2} = k\delta^{3/2}, \tag{10}$$

where δ represents the overlap of the spheres, k the normal stiffness, E^* the equivalent elastic modulus is given by

$$E^* = 1/((1-\nu_1^2)/E_1 + (1-\nu_2^2)/E_2). \tag{11}$$

E_1 and E_2 are the moduli of elasticity of the colliding bodies and ν_1 and ν_2 their Poisson ratios. The relative curvature R^* is defined as

$$R^* = \frac{1}{(1/R_1 + 1/R_2)}. \tag{12}$$

Only R^* differs between the pendulum and the UTS measurement. A straightforward computation yields (with the radius of curvature of rubber ball and impactor respectively

0.0415 and 0.025 m):

$$k_{pendulum} = 0.63\ k_{uts}. \tag{13}$$

The stiffness of the rubber ball (k_{uts}) measured with the universal testing machine (UTS) was 733 196 $N/m^{3/2}$. The stiffness measured with the pendulum ($k_{pendulum}$) was 394 931 $N/m^{3/2}$ (three experimental quantities optimization). When the above formula (13) is used, $k_{pendulum}$ becomes 461 913 $N/m^{3/2}$.

The difference between these last two values is probably due to the fact that the impactor is not perfectly spherical. In fact the radius of curvature is varying rapidly from 2.5 cm in the centre of the contact area to approximately 1 cm at the outside.

In future research a new impactor with well-known radius of curvature will be used. Another explanation could be the possible deformation rate dependency of the stiffness factor k of the rubber ball.

Further, the theoretical difference in damping constant between UTS and pendulum measurement is given here. As mentioned by Kuwabara and Kono [10] the damping constant c is given by

$$c = 4/5D'[R_1R_2/(R_1 + R_2)]^{1/2}. \tag{14}$$

R_1 and R_2 the radii of curvature of the colliding bodies and D' a material parameter depending on the coefficients of bulk viscosity ξ and η. The factor D' is the same for the pendulum as for the UTS. Using the radius of curvature of the flat plate (∞) and radius of curvature of rubber ball and impactor respectively 0.0415 and 0.025 m, a straightforward calculation yields

$$c_{pendulum} = 0.63c_{uts} \tag{15}$$

The damping parameter of the rubber ball (c_{uts}) measured with the universal testing machine (UTS) was 1078 $kg\,m^{-1/2}\,s^{-1}$. The damping parameter measured with the pendulum ($c_{pendulum}$) was 681 $kg\,m^{-1/2}\,s^{-1}$ (three experimental quantities optimization). When the above formula (16) is used, $c_{pendulum}$ becomes 673 $kg\,m^{-1/2}\,s^{-1}$. The difference between the damping constant between UTS and pendulum measurement is only 4 $kg\,m^{-1/2}\,s^{-1}$.

3. Biological materials: results and discussion

The parameters (damping and stiffness) of the Kuwabara–Kono model (5) were estimated for apples, tomatoes and potatoes, based on the experimentally measured displacement, displacement rate and contact force.

Twenty Jonagold apples, Spanish tomatoes, and Bintje potatoes were used for the measurements. The apples, tomatoes and potatoes were cut in two. Each half was mounted on the anvil, resulting in 40 repetitions in total for each sample.

For the determination of contact force models of biological materials, it is important that the impact is beneath the critical impact level, i.e., the material does not yield, otherwise the impact behaviour of undamaged tissue and damaged tissue are mixed up in the measurement. Because the signal-to-noise ratio of the force sensor is higher for large impact velocities and the control of the impact velocity is more accurate, the impact energy was taken as high as possible without the risk

damaging the tissue. The impact energy for potatoes was 0.024 J, for apples 0.010 J and for tomatoes 0.006 J.

This impact energy level is below the critical impact level for apples and potatoes. For the same potato variety used in the experiments ('Bintje'), Baheri [5] stated that the critical impact energy is situated between 0.065 and 0.115 J. For McIntosh apples, Studman et al. [14] stated that the critical impact energy level is between 0.010 and 0.017 J. No data about critical drop height or critical impact energy is available for Jonagold apples. The lowest critical drop height for apples (all measured varieties) in a literature overview by Hyde [15] was 6 mm. Assuming an average apple weight of 200 g, this corresponds to an impact energy of 0.012 J, which is far beyond the impact energy level used in the experiment to determine the contact force parameters.

Experimental evidence showed that no damage has occurred during impact. According to the constant height multiple impact method (CHMI), developed by Bajema and Hyde [4], no tissue damage has occurred when the force versus time graph of a repeated impact with the same impact energy shows the same force versus time graph as the first impact. This was verified experimentally for potatoes and apples at the impact energy level used in the experiment to determine the contact force parameters.

In the literature there is no data available about critical impact levels or critical impact height for external bruising of tomatoes. The reason is that bruise detection of tomato fruit is difficult due to a lack of visible tissue discoloration.

The CHMI method, validated for apples and potatoes [4], was used to estimate the critical impact energy level of tomato fruits used in the experiment. Starting at an impact energy level of 0.0095 J a shift in the force–time curve of the second impact occurred, compared to the first one. This impact energy level was also the starting point of the sense of a dent on the impacting spot. However, the correlation between the force–time shift and real tomato cell debonding or cell rupture is not known. Further investigation is necessary to correlate cell damage with the force–time shift. In conclusion, no clear evidence was found that there was no cell damage at the impact energy level of 0.006 J, but the starting point of the force–time shift at 0.0095 J can be used as an indication for the lack of damage at the given impacts used to determine the contact force parameters.

In the cost function (8) the weights w_x, $w_{\dot{x}}$ and w_F were chosen to normalize the different terms ($w_q = 1/\langle q \rangle$). The results are summarised in Table 3. Figs. 7–9 compare experimental and simulated contact force, displacement and displacement rate of a typical potato impact.

The standard deviation of the parameter estimations of the biological materials seems to be quite high. Two possible explanations could be given. The differences can be caused by

Table 3
Kuwabara–Kono contact force model parameter estimation of apples, tomatoes and potatoes based on displacement, displacement rate and contact force

Sample	$\langle k \rangle \pm \sigma_k$ ($\mathrm{N\,m^{-3/2}}$)	$\langle c \rangle \pm \sigma_c$ ($\mathrm{kg\,m^{-1/2}\,s^{-1}}$)	Residual norm C^2
Apples	753 599 ± 133 165 (18%)	1524 ± 263 (17%)	87 ± 41
Tomatoes	141 326 ± 45 970 (33%)	680 ± 200 (29%)	16 ± 15
Potatoes	654 324 ± 207 983 (32%)	1587 ± 320 (20%)	77 ± 27

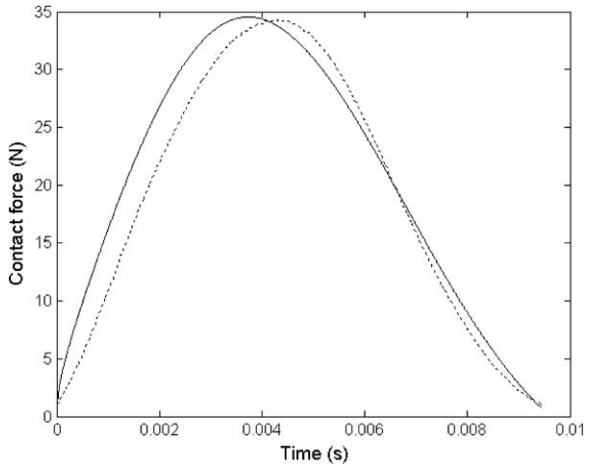

Fig. 7. Potato:experimental and simulated contact force with parameter estimation based on displacement, displacement rate and contact force. Solid line: simulation; Dotted line: experimental.

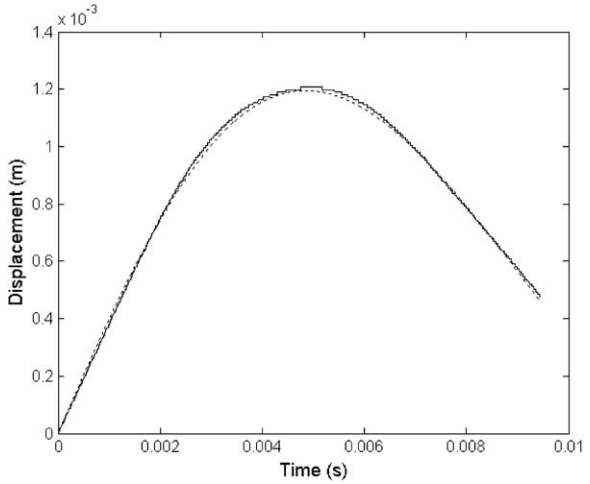

Fig. 8. Potato:experimental and simulated displacement with parameter estimation based on displacement, displacement rate and contact force. Solid line: simulation; Dotted line: experimental.

geometrical differences or by biological variability in mechanical tissue properties. Concerning the geometrical differences, in the methodology paragraph it was stated that the contact force (F_c) is also dependent of the radii of curvature of the colliding bodies (4). In future research the radii of curvature will be included in the model.

The higher standard deviation of the parameter estimations seen with potatoes than with apples and tomatoes can be explained by the more irregular shape of potatoes compared to apples and tomatoes. The higher standard deviation (percentage) of the parameter estimations of tomatoes

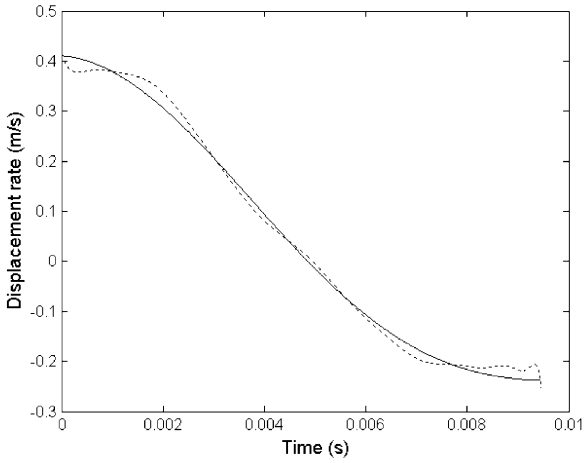

Fig. 9. Potato: experimental and simulated displacement rate with parameter estimation based on displacement, displacement rate and contact force. Solid line: simulation; Dotted line: experimental.

compared to apples could be explained by a possible higher anisotropy of tomato pericarp compared to apple flesh (literature comparison between apple and tomato morphology is rare).

4. Conclusions

An optical incremental encoder is an appropriate device to measure with high resolution and accuracy the displacement of the pendulum impactor. The same device makes it also possible to measure impact and rebound velocity of the impactor. Validation experiments making use of a rubber ball indicate that the experimental measurement of displacement, displacement rate and contact force (pendulum device) in combination with a Matlab optimization routine is an accurate method to estimate the parameters of a contact force model. The parameters of the Kuwabara–Kono model (5) were determined with success for apples, tomatoes and potatoes. Geometrical and biomechanical variation declares the rather high standard deviation in case of biological materials.

Acknowledgements

The authors wish to thank the former Federal Belgium Ministry of Small Trade and Agriculture for the financial support and B. Willems and D. Leroy for the technical assistance.

References

[1] E. Tijskens, H. Ramon, J. De Baerdemaeker, Discrete element modelling for process simulation in agriculture, *Journal for Sound and Vibration* 266 (3) (2003) 493–514, this issue.
[2] K.L. Johnson, *Contact Mechanics*, Cambridge University Press, Cambridge, 1987.

[3] C.W. Nelson, N.N. Mohsenin, Maximum allowable static and dynamic loads and effect of temperature for mechanical injury in apples, *Journal of Agricultural Engineering Research* 13 (1968) 305–317.
[4] R.W. Bajema, G.M. Hyde, Instrumented pendulum for impact characterization of whole fruit and vegetable samples, *Transactions of the ASAE* 4 (1998) 1399–1405.
[5] M. Baheri, Development of a Method for Prediction of Potato Mechanical Damage in the Chain of Mechanized Potato Production, Ph.D. Thesis Nr. 342, Faculty of Agricultural and Applied Biological Sciences, KU Leuven, Leuven, Belgium.
[6] G.-J. Molema, Mechanical Force and Subcutaneous Tissue Discolouration in Potato, Ph.D. Thesis, Wageningen University, Wageningen, The Netherlands, 1999.
[7] B.M. Nigg, W. Liu, The effect of muscle stiffness and damping on simulated impact force peaks during running, *Journal of Biomechanics* 32 (1999) 849–856.
[8] R.C. Fluck, E.M. Ahmed, Impact testing of fruits and vegetables, *Transactions of the ASAE* (1973) 660–666.
[9] C. Musiol, D. Harty, The use of numerical integration for the estimation of displacement from an accelerometer signal, Application note 12, nCode International Ltd., 1991.
[10] G. Kuwabara, K. Kono, Restitution coefficient in a collision between 2 spheres, *Japanese Journal of Applied Physics* 26 (8) (1987) 1230–1233.
[11] N.V. Brilliantov, F. Spahn, J.M. Hertzsch, T. Pöschel, Model for collisions in granular gases, *Physical Review E* 53 (3) (1996) 5382–5392.
[12] Y.H. Taguchi, Powder turbulence-direct onset of turbulent-flow, *Journal de Physique II* 2 (1992) 2103–2114.
[13] Y. Kishino, C. Thornton, Discrete element approaches, in: M. Oda, K. Iwashita (Eds.), *Mechanics of Granular Materials*, A.A. Balkema, Rotterdam, The Netherlands, 1999, pp. 147–223.
[14] C.J. Studmann, G.K. Brown, E.J. Timm, N.L. Schulte, M.J. Vreede, Bruising on blush and non-blush sides in apple-to-apple impacts, *Transactions of the ASAE* 40 (6) (1997) 1655–1663.
[15] G.M. Hyde, Advanced physical properties, 1998 http://www.wsu.edu/~gmhyde/ImpactProperties.html.